Model of water transfer in concrete and rock based on a single state variable to consider simultaneous positive pressure and drying boundary conditions

Aya Rima, Laurie Lacarrière, Alain Sellier, Ponleu Chhun, Minh-Ngoc Vu

Model of Water Transfer in Concrete and Rock based on a Single State Variable to Consider Simultaneous Positive Pressure and Drying Boundary Conditions

Authors

Aya Rima [(1)]*, Laurie Lacarrière [(1)], Alain Sellier [(1)], Ponleu Chhun [(1)], Minh-Ngoc Vu [(2)]

[(1)] Université de Toulouse, UPS, INSA, LMDC (Laboratoire Matériaux et Durabilité des Constructions), 135, avenue de Rangueil, 31 077 Toulouse Cedex 04, France

[(2)] Andra, 1-7 rue Jean Monnet, Chatenay Malabry, 92298, France

Corresponding author

E-mail address: rima@insa-toulouse.fr (Aya Rima)

Keywords

Water transfer, Drying, Saturation, Temperature, Concrete, Soil, Underground nuclear waste disposal.

Abstract

During their service life, concrete structures may be subjected to positive pressure and drying boundary conditions simultaneously. This phenomenon is likely to occur in civil engineering structures, such as tunnels for nuclear waste storage, dams, and piles, where the simultaneous phenomena of drying and saturation must be considered because of their strong effects on the short- and long-term behavior of the structure. The water transport model proposed in this paper predicts the mass transfer and water field in the material. It provides a continuous description of saturated and unsaturated media using liquid pressure as the only state variable and also considers the effects of temperature variations. A formulation for water transfer with a single state variable is presented, followed by an illustration of its numerical implementation and a procedure for the calibration of parameters. The model is compared with experimental and numerical results to validate its efficiency. For this purpose, several applications dealing with drying and saturation phenomena are used. The

Nomenclature

ϕ Porosity (-)

p_l Liquid pressure (Pa)

p_g Gas pressure (Pa)

p_v Vapor pressure (Pa)

p_c Capillary pressure (Pa)

p_{atm} Atmospheric pressure (Pa)

m_l Liquid mass (kg/m^3)

m_v Vapor mass (kg/m^3)

m_a Air mass (kg/m^3)

w_l Liquid mass flux $(kg/(m^2.s))$

w_v Vapor mass flux $(kg/(m^2.s))$

w_a Air mass flux $(kg/(m^2.s))$

$\vec{v_l}$ Liquid velocity (m/s)

$\vec{v_v}$ Vapor velocity (m/s)

S_l Liquid saturation (-)

RH Relative humidity (%)

ρ_l Fluid density (kg/m^3)

ρ_{ref} Reference fluid density (kg/m^3)

k_l Liquid permeability (m^2)

k_g Gas permeability (m^2)

k_{rl} Relative liquid permeability $(-)$

k_{rg} Relative gas permeability $(-)$

η_l Liquid dynamic viscosity $(Pa.s)$

η_g Gas dynamic viscosity $(Pa.s)$

M_{shr} Van Genuchten constant (Pa)

m_{vgn} Van Genuchten parameter (-)

n_{vgn} Van Genuchten parameter (-)

q Exponent of relative permeability to liquid (-)

p Exponent of relative permeability to gas (-)

k_w Liquid water bulk modulus (Pa)

T Temperature (K)

T_{ref} Reference temperature (K)

θ Temperature $(°C)$

λ thermal conductivity $(W/(m.K)$

λ_{ref} Reference thermal conductivity $(W/(m.K)$

C_p Heat capacity $J/(kg.K)$

$C_{p\ ref}$ Reference heat capacity $J/(kg.K)$

h Convection coefficient $(W/m^2.°C)$

results obtained show the potential of the proposed water transfer model to evaluate the water transport in the material under study at different temperatures by simulating a mock-up of nuclear power plant wall. It is finally used to predict the re-saturation of an underground nuclear waste disposal structure.

1 Introduction

In civil engineering structures, it is essential to understand the behavior of construction materials from the time of placement through long-term use. The most commonly used construction material for buildings and structures is concrete, and water is an important factor affecting its characteristics and behavior due to its porosity. It is, therefore, necessary to understand the movement of moisture in concrete structures over time. In such structures, the influence of various phenomena on their behavior must be taken into account. One of these phenomena is the significant condensation of vapor that occurs when the structure is rapidly exposed

to high temperatures, conditions that can be found in concrete walls of containment vessels in case of a severe accident (interior temperature rising to 200 °C in a matter of minutes). In some cases, the structure investigated may also be partially immersed in water (as in the case of dams, pile foundations, and deep underground nuclear waste repository). For this reason, the coexistence of saturated and unsaturated zones must be considered when studying water transfer in concrete structural elements.

The phenomenon of water transport in porous media at high temperatures is a topic of considerable concern. The importance of coupled models involving heat transfer, liquid water flow, and gaseous water flow to describe the short- and long-term behavior of concrete subjected to temperature rise has been emphasized by various researchers. Theoretically, Richards' formulation can be used to describe the motion of water in porous materials [Richards, 1931]. However, due to its non-linearity, large mass balance and convergence problems can be encountered. [Philip and De Vries, 1957] and [Luikov, 1975] were among the first authors to propose the pioneering models of coupled partial differential equations governing heat and moisture in a porous material. Based on these theoretical models, [Bažant and Thonguthai, 1978; Gong et al., 1991] proposed a mathematical model to describe the drying process of concrete. Recent work, derived from the model proposed by [Philip and De Vries, 1957], to study the transport of heat, water and salt can also be found [Zhang et al., 2023].

Another water transfer model is proposed in [Bažant and Najjar, 1971]. It is based on solving a nonlinear diffusion equation. In that model, the water content is the state variable and the water diffusion coefficient is calculated as a function of the water content. This approach has been used by several researchers, such as [Mensi et al., 1988]. Other works using the same concept but replacing water content by relative humidity degree of saturation can also be found in [Xi et al., 1994; Witasse et al., 2002; Šmilauer et al., 2019; Carette et al., 2020]. However, the hydric diffusion coefficient includes the movements of both vapor and liquid water. Thus, it is difficult to evaluate the importance of each phenomenon using only this coefficient.

More complex modeling of the water transport in the porous medium can be found in [Baroghel-Bouny et al., 1999; Gawin et al., 1999; Mainguy et al., 2001; Thiery et al., 2007; Pohl et al., 2021]. These models involve the interaction of three phases: liquid water, water vapor, and dry air. The main strength of these models is that they take account of all the important phenomena in porous media, such as vapor diffusion, liquid water flow due to pressure gradients and capillary effects, evaporation/condensation phenomena, etc. However, in these models, the contribution of coupling between mechanisms is assumed to be weak.

Most of the available numerical codes provide a quasi-multi-physical calculation in which three conservation

equations are treated as coupled (liquid mass, vapor mass, and dry air mass). Consequently, three state variables are treated simultaneously, which complicates the numerical implementation and the solving process in non-linear contexts.

In the present work, the main objective is to reduce the number of conservation equations to be solved in order to obtain a single state variable formulation. This simplifies the problem of calculating water pressure in concrete simultaneously subjected to positive and negative pressures at its boundary conditions. Such a transfer model is proposed and validated here. Special attention is paid to the ability of the model to provide continuity between saturated and unsaturated media through a single state variable. Section 2 describes the constitutive model and governing equation for water transfer. Section 3 details the numerical implementation and the coupling with the heat transfer calculation. The calibration methodology of the model parameters is presented in Section 4 and several numerical simulations are performed using the proposed water transfer model to calibrate, validate, and finally to predict the long term re-saturation of an underground concrete structure. Finally,conclusions and perspectives are presented in Section 5.

2 Constitutive Model

2.1 Governing Equation for Water Mass Transfer

Moisture migration mechanisms in porous media, such as concrete, are mainly controlled by the porosity of the material. In these materials, water movement can be in liquid, vaporous or gaseous form. The study and understanding of these transports require the coupling between the conservation equations of the different phases present in the porous medium. Generally, the phases are constituted of the liquid phase and the gaseous phase. The liquid phase is formed by water and the gas phase includes water vapor and dry air. The conservation equations also involve the exchange of water between solids and liquids as well as the phenomena of vaporization and condensation. The system of conservation equations is expressed as follows:

$$\begin{cases} \dfrac{\partial m_l}{\partial t} = -div(\vec{w_l}) + S_{(v)\to(l)} + S_{(s)\to(l)} \\ \dfrac{\partial m_v}{\partial t} = -div(\vec{w_v}) - S_{(v)\to(l)} \\ \dfrac{\partial m_a}{\partial t} = -div(\vec{w_a}) \end{cases} \tag{1}$$

with m_i the mass quantity per m^3 of material, w_i the mass flux and i the index corresponding to liquid water (l), water vapor (v), or air (a). $S_{(v)\to(l)}$ and $S_{(s)\to(l)}$ are, respectively, the amount of mass exchanged by

vaporization/condensation and the amount of mass exchanged due to the phase change from solid to liquid (as, for example, in the case of hydration or dehydration).

According to system (1), to solve the hydric transfer problem, three conservation equations of three state variables (m_l, m_v, m_a) must be solved. However, in some conditions, it is possible to reduce the number of equations in order to simplify the model and reduce the computational cost. Two possible types of simplification are to be found in the literature:

- A first approach, used to model drying at room temperature, assumes that the gas pressure, p_g, is in equilibrium with atmospheric pressure, p_{atm} ($p_g = p_{atm}$) [Mainguy et al., 1999]. They assume that the gas in the pores always has time to be balanced with the outside. This assumption is only valid at room temperature and when the structure is thin. Otherwise, the gas vapor does not have time to evacuate and to re-equilibrate with the atmospheric pressure. In massive structures submitted to a rapid temperature rising, since heat transfer is faster than gaz permeability the water evaporates but its evacuation is not rapid enough to apply the [Mainguy et al., 1999] assumption.

- A second approach, used to model water transfer during heating, considers that the gas consists only of vapor. Consequently, the gas pressure, p_g, is equal to the vapor pressure, p_v ($p_g = p_v$) [Bary et al., 2012; de Morais et al., 2009]. This approach assumes that the liquid water stored in the small pores supplies enough vapor to control the gas pressure.

In the present paper, the materials are porous and initially partially desaturated (high initial relative humidity). These types of materials contain pores of different sizes. At high initial relative humidity, it is assumed that the fine pores are saturated with liquid water and the large pores are formed by a mix of vapor and dry air. When the temperature rises rapidly, the mix in the large pores is first evacuated. The large pores are then supplied with vapor by the inter-connected saturated small pores. At this stage, the small pores begin to desaturate. As time passes, they desaturate more and more and the porosity becomes controlled by the vapor pressure. This phenomenon makes it possible to simplify the problem and neglect the dry air amount initially present in large pores when compared with the amount of vapor coming from liquid of small pores evaporation. So, in this work the second approach is adopted and it is assumed that the contribution of dry air pressure, p_a, can be negligible compared to the vapor pressure, p_v. Consequently the gas pressure, p_g, is assimilated to the vapor one. This assumption allows the air mass, m_a, to be neglected. Thus, the third equation of system (1) can be eliminated and the two mass conservation equations of water in the liquid and gas phases can be added to create a single balance equation [Richards, 1931; Mainguy et al., 1999; Bary et al., 2008; Ranc et al., 2003].

Consequently, the single mass conservation equation is expressed in the following form:

$$\frac{\partial(m_l + m_v)}{\partial t} = -div(\vec{w_l} + \vec{w_v}) + S_{(s)\to(l)} \tag{2}$$

The quantity of mass, m_i, is given as a function of its density, ρ_i, water saturation, S_l, and porosity, ϕ by:

$$m_l = \rho_l \ \phi \ S_l \tag{3}$$

$$m_v = \rho_v \ \phi \ (1 - S_l) \tag{4}$$

It is worth noting that, in this work, there is no chemical evolution leading to variation of the porosity over time. Thus, a constant porosity is expected in the material ($\phi = \phi_0$).

Assuming that the vapor behaves like an ideal gas, its density, ρ_v, can be expressed by the ideal gas equation (Equation 5), in which p_v is the vapor pressure, M_v is the molar mass ($0.018\ kg/mol$ for water), R is the universal gas constant ($8.314\ J/mol.K$), and T is the temperature.

$$\rho_v = \frac{p_v \ M_v}{R \ T} \tag{5}$$

For each phase, the mass flux $\vec{w_i}$ is considered as the product of the density, ρ_i, and the transfer velocity, $\vec{v_i}$ (Equation 6).

$$\vec{w_i} = \rho_i * \vec{v_i} \tag{6}$$

Both velocities $\vec{v_l}$ and $\vec{v_v}$ are assumed to be mainly controlled by the pressure gradient p_i and are expressed by Darcy's law. On the other hand, the Klinkenberg coefficient, Γ, is added to the expression of the vapor velocity $\vec{v_v}$ in order to take account of the gas transfer relative to the molecular flow [Klinkenberg, 1941]. The liquid and vapor velocities are expressed as follows:

$$\vec{v_l} = -\frac{k_l}{\eta_l} \ k_{rl} \ \vec{grad} \ p_l \tag{7}$$

$$\vec{v_v} = -\frac{k_g}{\eta_g} \ k_{rg} \ \left(1 + \frac{\Gamma}{p_v}\right) \ \vec{grad} \ p_v \tag{8}$$

with k_i $(i = l,\ g)$ the intrinsic permeability of concrete, η_i $(i = l,\ g)$ the dynamic viscosity of liquid/gas, k_{ri} $(i = l,\ g)$ the relative permeability of concrete to the liquid/gas, and Γ the Klinkenberg coefficient.

2.2 Single State Variable Hydric Model in Saturated and Unsaturated Porous Media

In a porous medium, it is important to distinguish between a saturated and an unsaturated medium when studying the water mass transfer. Specifically, the vapor pressure existing in a partially saturated porous medium is not present in a saturated condition. Accordingly, only the liquid mass is taken into account in the moisture transfer equation when the medium is saturated. Moreover, the liquid pressure is based on the same physical phenomena in these two zones. In the saturated zones, the pressure is mainly driven by the bulk modulus of water while, in the unsaturated zones, the pressure is controlled by the water retention curves. Note that the mass exchange due to the phase change from solid to liquid $S_{(s)\rightarrow(l)}$ is neglected in this study (hardened concrete and environmental conditions that do not lead to dehydration).

2.2.1 Saturated Media

As previously indicated, in the case of a saturated porous medium, the moisture transport is exclusively liquid and will depend only on the liquid pressure p_l. This pressure is expressed as a function of the mass of liquid water entering the representative volume according to the following law:

$$p_l = k_w \left(\frac{m_l}{\rho_l} - \phi \right) \tag{9}$$

where k_w is the liquid water bulk modulus. Note that, in this work and for sake of simplification, the solid is considered as undeformable. Also, as mentioned in Section 2.1, chemical evolution, which would result in a constant porosity in the material ($\frac{\partial \phi}{\partial t}$=0), is not included in this study. Thus, the conservation equation of the water mass in saturated condition (Equation 2), combined with liquid pressure equation (Equation 9) becomes:

$$\rho_l \frac{1}{k_w} \frac{\partial p_l}{\partial t} = div \left(\frac{k_l}{\eta_l} \; \rho_l \; \vec{grad} \; p_l \right) \tag{10}$$

Note that the assumption of undeformable solid matrix is not strictly necessary, and can be replaced by the Biot poro-mechanical formulation in the case of coupling with continuum mechanics of porous solids [Coussy, 2004].

2.2.2 Unsaturated Media

In partially saturated media, where the degree of saturation varies between 0 and 1, thermodynamic equilibrium such as described by the Kelvin-Laplace law and isothermal sorption curves, as well as Darcy's equation, are

applicable to the liquid and vapor phases. Assuming that the gas phase is composed of only vapor, the liquid and vapor transfers can be combined into a single model, as presented in Section 2.1. The following equilibrium equation is recalled from the governing equation (Equation 2). The first term represents the change in mass quantities of liquid and vapor and the second term is the mass flow balance resulting from the transfer of liquid and vapor under gradients of pressures.

$$\frac{\partial}{\partial t}\left(\rho_l\ \phi\ S_l + \frac{p_v M_v}{RT}\phi(1-S_l)\right) = div\left(\rho_l \frac{k_l}{\eta_l} k_{rl}\ \vec{grad}\ p_l + \frac{p_v M_v}{RT}\frac{k_g}{\eta_g}k_{rg}\left(1+\frac{\Gamma}{p_v}\right)\ \vec{grad}\ p_v\right) \tag{11}$$

2.3 Choice of the State Variable

In the context of the applicability of the hydric model developed here to structures, the co-existence of zones under a positive pressure and of unsaturated zones must be considered, as in the case of problems simultaneously presenting a boundary condition of drying and another one in contact with a positive liquid pressure (dams, ventilated tunnel in a submerged area, etc.). The conservation equation of the partially unsaturated medium (Equation 11) is written in terms of three state variables (p_l, p_v, and S_l). Each of these three variables can then be chosen as the state variable, while the other two become internal variables and are expressed in terms of the chosen state variable.

The vapor pressure, p_v, and the degree of saturation, S_l, are defined respectively by thermodynamic equilibrium, such as in the Kelvin-Laplace law, and water retention curves. These are useful while the material is in a partially saturated state, precluding transfer to the saturated condition (absence of vapor in the porosity).

In the water transfer model proposed by [Bary et al., 2012], the negative pressure of the liquid, p_l, is chosen as state variable of the problem and is expressed as a function of the capillary pressure. As a result, only partially saturated zones can be modeled and liquid over-pressure cannot be taken into account. This limitation is critical for our case study. This is the reason why an extension of the hydric model of [Bary et al., 2012] is proposed in this paper. This extended formulation has to be able to handle both drying and over-pressure conditions simultaneously. Therefore, in this work, the liquid pressure p_l is selected as the state variable to capture the over-pressure of the liquid water. The main advantage of this choice is that the liquid pressure, p_l, can vary from a positive value, when the medium is saturated, to a negative value, when it is not, thus ensuring continuity from one state to another.

The governing equation for mass transfer in an unsaturated medium (Equation 11) becomes:

$$\left[\rho_l\ \phi\ \frac{\partial S_l}{\partial p_l} + \frac{M_v}{RT}\phi\frac{\partial\left(p_v(1-S_l)\right)}{\partial p_l}\right]\ \frac{\partial p_l}{\partial t} = div\left(\left[\rho_l\frac{k_l}{\eta_l}k_{rl}\ + \frac{p_v M_v}{RT}\frac{k_g}{\eta_g}k_{rg}\left(1+\frac{\Gamma}{p_v}\right)\ \frac{\partial p_v}{\partial p_l}\right]\ \vec{grad}\ p_l\right) \tag{12}$$

It can be seen that Equation 12 involves the vapor pressure, p_v, and the degree of saturation, S_l, together with

their partial derivation with respect to the liquid pressure, p_l. To formulate this equation with only the chosen state variable, p_v and S_l must be written in terms of p_l. The relation between p_l and $p_v(T, P_l)$ is derived from the Kelvin-Laplace law. The degree of saturation $S_l(T, P_l)$ is given as a function of the capillary pressure, p_c, and the temperature, T, by an analytical expression deduced, for instance, from [Van Genuchten, 1980].

2.3.1 Relationship between p_v and p_l

For the purpose of writing Equation 12 for a partially saturated condition using only the state variable p_l, it is feasible to replace p_v by p_l via the Kelvin-Laplace law.

The capillary pressure, p_c, is related to the vapor pressure, p_v, and saturated vapor pressure, p_{vs}, through the law of Kelvin-Laplace, by which gas pressure, p_g, and liquid pressure, p_l, are in equilibrium. Since the dry air mass is assumed to be negligible, the gas pressure, p_g, can be replaced by p_v. Thus, the equation for the capillary pressure has the following form:

$$p_c = p_g - p_l \approx p_v - p_l = -\rho_l \frac{RT}{M_v} ln\left(\frac{p_v}{p_{vs}}\right) \tag{13}$$

with M_v the molar mass of water, R the gas constant, and ρ_l the density of liquid water.

It is impossible to invert the relation in Equation 13 analytically to obtain an expression for p_v as a function of p_l. This is because the solution of this equation depends on the Lambert W-function, which gives an infinite series, so the analytical solution does not exist. To overcome this difficulty, it is important to find an analytical form for the internal variable p_v as a function of p_l. Since the capillary pressure, p_c, is the difference between the vapor pressure, p_v, and the liquid pressure, p_l, its derivation can be written as follows:

$$dp_c = dp_v - dp_l \tag{14}$$

At constant temperature and due to the equilibrium between liquid and gas, the variation of the chemical potential is given by [Barrett et al., 1951]:

$$V_{v,mol}\ dp_v = V_{l,mol}\ dp_l \tag{15}$$

Assuming that the molar volume of the liquid, $V_{l,mol}$, is not negligible compared to the molar volume of the vapor, $V_{v,mol}$, the derivation of the capillary pressure, p_c, expression becomes:

$$dp_v - \frac{V_{v,mol}}{V_{l,mol}} dp_v = dp_c \tag{16}$$

By supposing that the vapor phase behaves as an ideal gas and by replacing $V_{l,mol}$ and $V_{v,mol}$ by their expressions, Equation 16 becomes:

$$dp_v - \frac{\rho_l RT}{M_v}\frac{dp_v}{p_v} = dp_c \tag{17}$$

Since in an unsaturated medium, the vapor pressure can have a peak value equal to p_{vs}, the integration of Equation 17 gives:

$$\int_{p_{vs}}^{p_v} dp_v - \int_{p_{vs}}^{p_v} \frac{\rho_l RT}{M_v}\frac{dp_v}{p_v} = \int_0^{p_c} dp_c \tag{18}$$

Consequently, the expression obtained has an exponential form that respects the Kelvin-Laplace law whatever the temperature (Equation 19).

$$p_v = p_{vs}\ \exp\left(\frac{M_v}{\rho_l RT}\ (p_l - p_{vs})\right) \tag{19}$$

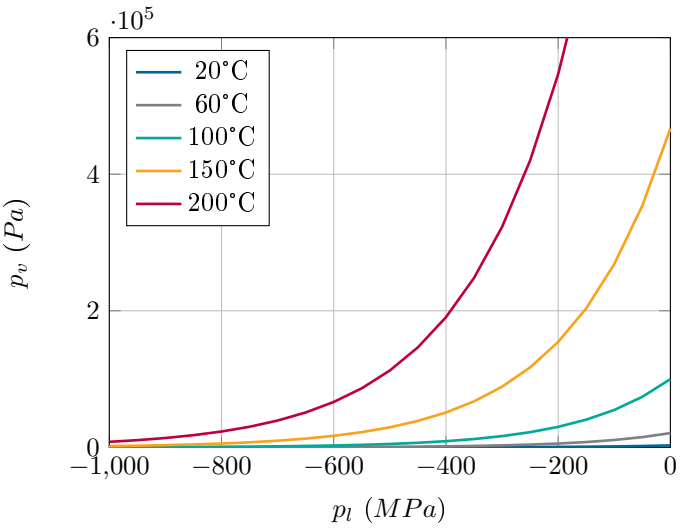

Figure 1: Relation $p_v(T, p_l)$ for different temperatures.

2.3.2 Relation between S_l and p_l

The expression for the degree of saturation S_l as a function of RH is given experimentally by the water retention curves; the use of Kelvin's law then allows S_l and P_l to be related. The hysteresis between the sorption and desorption branches of these curves could be considered but, as the aim here is not to describe the problem of hysteresis, and for the sake of simplification, hysteresis is not treated in this paper. Since the degree of saturation, S_l, depends strongly on the temperature, its influence must be included. An analytical expression,

derived from [Van Genuchten, 1980], is proposed (Equation 20).

$$S_l = \left[1 + \left(\frac{p_c}{M_{shr}}\right)^{n_{vgn}}\right]^{-m_{vgn}} \tag{20}$$

with n_{vgn} and m_{vgn} the Van Genuchten exponents and M_{shr} a parameter that takes the influence of the temperature into account. These parameters are used to calibrate the numerical curves on the basis of experimental data for a range of temperatures. Regarding M_{shr}, an exponential form is proposed that depends on only two parameters: M_{shr0} measured at a reference temperature (T_{ref} = 20 °C) and T_{kvgn} calibrated to fit M_{shr} to the experimental results (Equation 21).

$$M_{shr}(T) = M_{shr0}\ exp\left(-\frac{T - T_{ref}}{T_{kvgn} - T_{ref}}\right) \tag{21}$$

Figure 2 illustrates the evolution of the degree of saturation S_l as a function of the liquid pressure p_l using the analytical expression of Equation 20. For this figure, the values of n_{vgn}, m_{vgn}, M_{shr}, and T_{kvgn} are taken to be 1.35, 0.26, 10 MPa, and 40 °C respectively. It can be seen that, for a given liquid pressure, p_l, the degree of saturation S_l decreases with temperature increase. At high temperature and when p_l is almost equal to 0, S_l presents a sharp slope for a small variation of p_l and evolves strongly in this area.

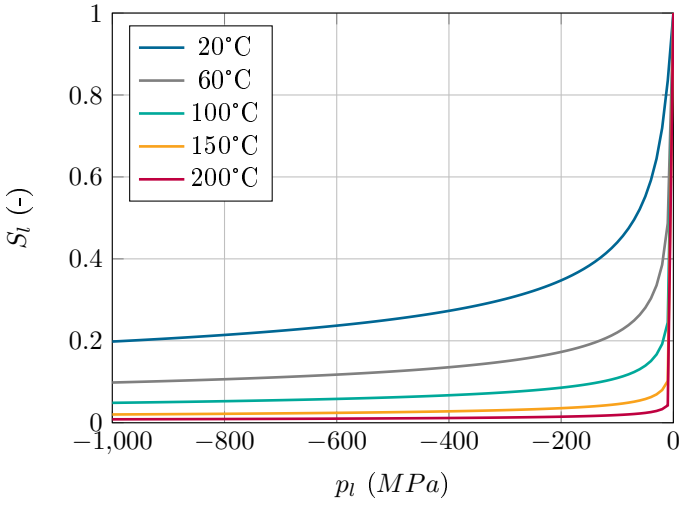

Figure 2: Evolution of S_l (-) in function of p_l (MPa) for different temperatures.

Hence, using Equations 19 and 20, the conservation equation can be solved using p_l as a continuous state variable for the partially saturated and saturated conditions.

2.4 Hydric Balance Equation

As stated previously, the liquid pressure p_l is chosen as the only state variable when solving hydric problems. The major strength of the proposed water transfer model is that it allows the transition from an unsaturated state to a saturated state and vice versa by providing continuity between the two.

The hydric equilibrium equation used in the numerical study is presented in Equation 22.

$$C_l \frac{\partial p_l}{\partial t} = div(K_l \vec{grad}\ p_l) \tag{22}$$

Only the coefficients C_l and K_l of the equation depend on the pressure but, since the form of the equation supports both negative (unsaturated) and positive (saturated) pressures, the goal of having a single form of partial differential equation is achieved. Of course, when solving numerically by the finite element method, the coefficients of this equation will have to be continuously updated to the pressure level at each Gauss point, which will require an iterative process in case of implicit formulation. The expressions of theses coefficients are summarized depending on the pressure value.

2.4.1 Terms for the Unsaturated Case

In a partially saturated medium, the two coefficients C_l and K_l can be deduced by replacing Equations 19 and 20 in the mass conservation equation (Equation 2). They are given by:

$$C_l = \left(\rho_l - \frac{p_v M_v}{RT}\right) \frac{m_{vgn}\ n_{vgn}}{M_{shr}} \phi \left[1 + \left(\frac{p_c}{M_{shr}}\right)^{n_{vgn}}\right]^{-m_{vgn}-1} \left(\frac{p_c}{M_{shr}}\right)^{n_{vgn}-1} + \frac{\phi}{\rho_l}\left(\frac{M_v}{RT}\right)^2 (1 - S_l) p_v \tag{23}$$

$$K_l = \rho_l \frac{k_l}{\eta_l}\ k_{rl} + \frac{1}{\rho_l}\left(\frac{p_v M_v}{RT}\right)^2 \frac{k_g}{\eta_g} k_{rg} \left(1 + \frac{\Gamma}{p_v}\right) \tag{24}$$

As shown in Equation 24, the mass permeability coefficient, K_l, is the sum of two terms combining the different phases of moisture transport. The first term is related to the Darcy transport of moisture in liquid form, while the second includes the diffusive transport of moisture in gaseous form. These two modes of moisture transfer are coupled and occur simultaneously in unsaturated conditions.

2.4.2 Terms for the Saturated Case

For the saturated condition, and based on Equation 10, the coefficients C_l and K_l become:

$$C_l = \frac{\rho_l}{k_w} \tag{25}$$

$$K_l = \rho_l \frac{k_l}{\eta_l} \tag{26}$$

It can be seen from Figure 3 that the proposed hydric transfer model can manage both saturated and unsaturated conditions by providing a continuous description and using only one state variable.

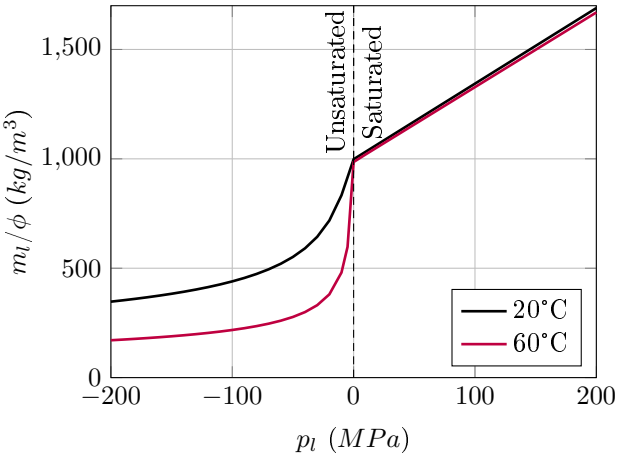

Figure 3: Continuous description of the hydric model for saturated-unsaturated media at 20°C and 60°C.

2.5 Evolution of Hydric Parameters

Almost all the parameters involved in the previous equations depend on temperature or saturation. Although these dependencies are known for most terms, this section recalls their laws of evolution, and Table 1 summarizes the constants to be used for each of these terms.

Relative Permeability

In the partially saturated condition, it can be seen that the permeability coefficient K_l (Equation 24) depends strongly on the liquid saturation of the material through the evolution of the relative permeability k_{ri} $(i = l, g)$ as a function of the saturation degree, S_l. The relative permeabilities to liquid, k_{rl}, and gas, k_{rg}, are introduced to describe the macroscopic effect of the porous distribution and connectivity of the cement paste. The analytical expressions used to relate the relative permeability to the degree of saturation are those proposed

by [Van Genuchten, 1980]. They can be given by the following expressions:

$$k_{rg}(S_l) = (1 - S_l)^p (1 - S_l^{\frac{1}{m_{vgn}}})^{2m_{vgn}} \qquad (-) \tag{27}$$

$$k_{rl}(S_l) = S_l^q \left[1 - (1 - S_l^{\frac{1}{m_{vgn}}})^{m_{vgn}}\right]^2 \qquad (-) \tag{28}$$

where p and q are fitting parameters controlling the isothermal sorption curve of concrete. It is usual in the literature to find a coefficient q equal to 0.5 and p varying between 3.5 and 5.5. When the porous medium is saturated ($S_l = 1$), k_{rl} and k_{rg} become equal to 1 and 0, respectively. Conversely, when S_l tends to 0, the value of k_{rl} approaches 0 and k_{rg} becomes equal to 1.

Dynamic Viscosity

The dynamic viscosity of the liquid, η_l, and the dynamic viscosity of the vapor, η_g, employed in the hydric transfer equation for both the saturated and unsaturated conditions (Equation 24 and 26) are defined by analytical expressions based on experimental results. For η_l, an empirical expression is proposed in [Thomas and Sansom, 1995] depending on the temperature. Similarly, an expression for the dynamic viscosity of vapor, η_g, is provided in [Feraille-Fresnet, 2000]. The dynamic viscosity expressions are given as follows:

$$\eta_l(T) = \kappa_{\eta l}(T - T_{K\eta})^{\zeta_\eta} \qquad (Pa.s) \tag{29}$$

$$\eta_g(T) = \kappa_{\eta g}\, T \qquad (Pa.s) \tag{30}$$

with $\kappa_{\eta l}$, $T_{K\eta}$, ζ_η, and $\kappa_{\eta g}$ equal to 0.6612 $Pa.s/K^{\zeta_\eta}$, 229 K, -1.562, and 3.85*10^{-5} $Pa.s/K$, respectively.

Liquid Density

In a porous material such as concrete, the presence of water is a critical factor in water transfer. As a consequence of thermal expansion, the density of the liquid decreases as the temperature increases. In this work, the expression for the liquid density, ρ_l, proposed by [Raznjevic and Podhorsky, 1970] and based on experimental data, is used (Equation 31).

$$\rho_l = \rho_K + \rho_T \left[1 - \left(\frac{\theta}{\theta_K}\right)^{\frac{1}{\zeta_l}}\right]^{\zeta_l} \qquad (kg/m^3) \tag{31}$$

where ρ_K, ρ_T, θ_K and ζ_l are equal to 314.4 kg/m^3, 685.6 kg/m^3, 374.14 $°C$ and 0.55, respectively.

Saturated Vapor Pressure

The saturated vapor pressure, p_{vs}, depends only on temperature. It increases with temperature. The model used to estimate the evolution of p_{vs} with temperature is the one suggested by [Bary et al., 2012] and is based on the Arrhenius equation [Arrhenius, 1900].

$$p_{vs}(T) = p_{atm}\ exp\left[\frac{E_a}{R}\left(\frac{1}{T_b} - \frac{1}{T}\right)\right] \qquad (Pa) \tag{32}$$

where E_a is the activation energy and is given as 40500 J/mol. T_b is the boiling temperature of the substance at p_{atm}. For water, it is equal to 100°C.

Klinkenberg Coefficient

The Klinkenberg coefficient, Γ, used to express the vapor velocity in Equation 8, varies with the degree of saturation S_l. A significant decrease in this value occurs as the degree of saturation increases. A linear form of Γ is provided in [Kameche et al., 2014].

$$\Gamma(S_l) = \Gamma_0\ (1 - S_l) \qquad (Pa) \tag{33}$$

with Γ_0 equal to 3.12*10^5 Pa.

2.6 Table of Constants

The set of constant values used in the model equations is summarized in Table 1.

Table 1: Constants used in the model.

Symbol	Value	Unit
M_v	0.018	kg/mol
R	8.314	$J/mol.K$
k_w	2.22	GPa
p_{atm}	10^5	Pa
$\kappa_{\eta l}$	0.6612	$Pa.s/K^{\zeta_\eta}$
$T_{K\eta}$	229	K
ζ_η	-1.562	-
$\kappa_{\eta g}$	$3.85e^{-8}$	$Pa.s/K$
ρ_K	314.4	kg/m^3
ρ_T	685.6	kg/m^3
θ_K	374.14	$°C$
E_a	40500	J/mol
Γ_0	$3.12e^5$	-

3 Numerical Implementation (Thermo-Hydric model)

When the behavior of moisture transport is described in a porous material such as concrete, the temperature evolution must be taken into account. For this purpose, the coupling between temperature and moisture needs to be considered and a thermo-hydric model is required. For the thermal equation, the temperature, T, can be kept as a classical state variable used to solve the heat balance equation. However, for the water transfer, the case is much more complicated. The two governing equations for the thermal and water problem are:

$$C_T(T)\ \frac{\partial T}{\partial t} = div(\lambda(T)\ \vec{grad}\ T) \tag{34}$$

$$C_l(p_l, T)\ \frac{\partial p_l}{\partial t} = div(K_l(p_l, T)\ \vec{grad}\ p_l) \tag{35}$$

where $\lambda(T)$ is the thermal conductivity and $C_T(T)$ is the thermal capacity given by the amount of heat required to change the temperature. It is also given by the product of the material's density ρ and the heat capacity, c_p, $(C_T = \rho.c_p)$.

In this type of chained formulation, the effect of water on the heat flows is approximated by a capacity and a conductivity that are phenomenologically dependent on T. In reality, the specific capacity and the thermal conductivity of a heat transfer problem should be a function of water content but, as with concrete the amount of energy involved in the phase changes of water is relatively small with respect to the heat stored in the solid, variations in the coefficients of the heat equation remain small from one concrete to another. For this reason, expressions of capacitance and thermal conductivity as functions of temperature can be used, e.g. that proposed in [Eurocode2, 2004] for the fire design of structures.

Thus, in the present case, for the sake of simplification and because our objective is to reduce the problem of mass transfer and not that of the strong coupling with heat, the chained formulation is implemented. The main advantage is in the fact that the thermal problem is solved first, then the liquid pressure problem is tackled using the calculated temperature. Numerically, the thermo-hydric model equations are solved by the finite element method (FEM) using the Cast3M code [CEA, 2016]. The procedure for the hydric resolution is summarized in Figure 4. As mentioned previously, the state variables for the thermal problem and the hydric problem are temperature, T, and liquid pressure, p_l, respectively. Since the capacity, C_l, and the mass permeability, K_l, of the governing water equation depend on the temperature, T, and liquid pressure, p_l, they are updated at each iteration. Therefore, an implicit calculation is performed.

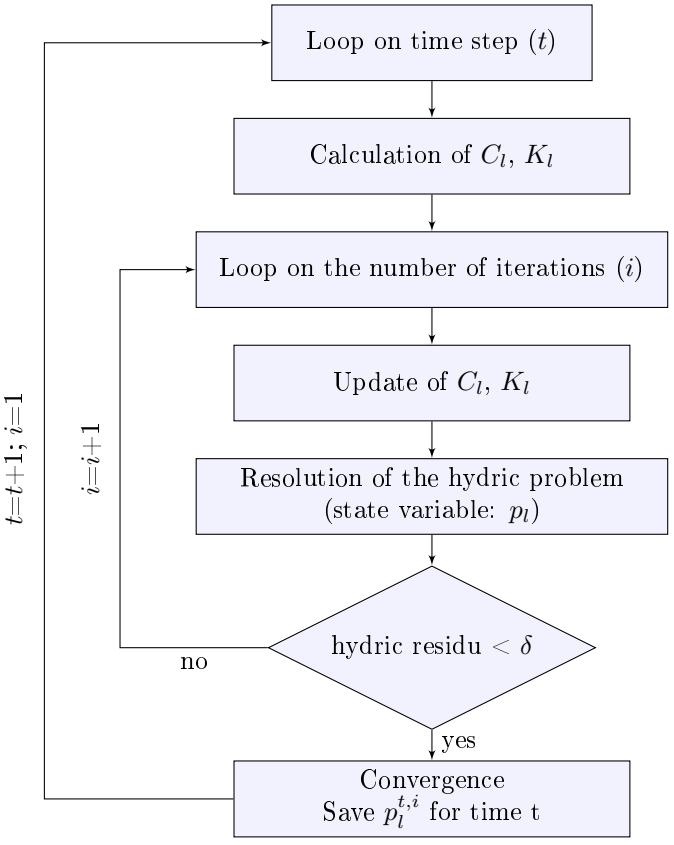

Figure 4: Scheme representing the hydric model resolution.

4 Calibration Methodology for Parameters Used in Unsaturated Problem

As the hydric model presented above depends on several parameters, a calibration step, based on experimental results, is required. This section deals with the identification and calibration of the different parameters of the proposed hydric transfer model. The calibration process uses an inverse analysis, a detailed explanation of which is provided to clarify the calibration methodology. The concrete used in this study is a classical clinker based one.

4.1 Desorption Isotherm Fitting

The desorption isotherm for concrete is approximated using the Van Genuchten expression (Equation 20). This is achieved by calibrating the parameters m_{vgn}, n_{vgn}, M_{shr} until the experimental isotherm of the concrete is obtained. As our goal is not to treat the problem of isotherm hysteresis, the hysteresis loop is not considered, and only the desorption branch is fitted. It can be seen from Figure 5 that the curves obtained from Van Genuchten's relation agree with the experimental points given in [Poyet, 2009; Ranaivomanana, 2010; Chen et al., 2012] for different temperatures. The parameters m_{vgn}, n_{vgn}, and M_{shr0} are set to 0.35, 1.1 and 13 MPa, respectively.

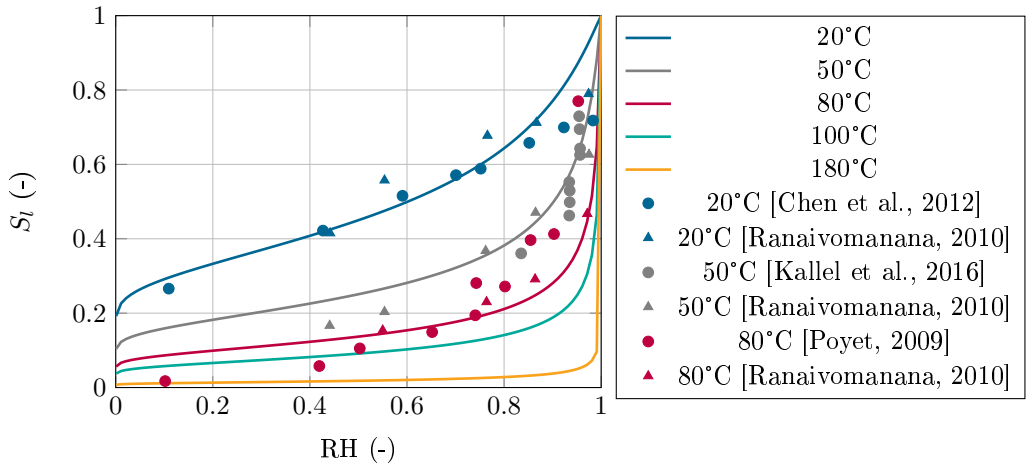

Figure 5: Influence of temperature on isothermal desorption curves (solid line: Equation 20, points: experimental results).

4.2 Identification of the Relative Permeabilities

Once the fitting parameters of the Van Genuchten expression have been found, the parameters p and q controlling the relative gas/liquid permeability are identified (Equations 27 and 28). The identification is based

on experimental studies found in the literature. Unlike for gas permeability, few experimental investigations on the liquid water permeability of partially saturated cement paste are available because of measurement difficulties. Figure 6 illustrates the experimental results (points) of the relative permeability of gas [Monlouis-Bonnaire et al., 2004] and liquid [Kameche et al., 2014] at 20°C. In the present work, the values of q and p are set to 0.5 and 4.5 according to the curves obtained with the numerical relative permeability models (Figure 6). Because there are not enough experimental points to calibrate the relative liquid permeability, k_{rl}, particular attention is paid only to the relative gas permeability, k_{rg}, and an inverse analysis of the following examples is performed to identify this parameter.

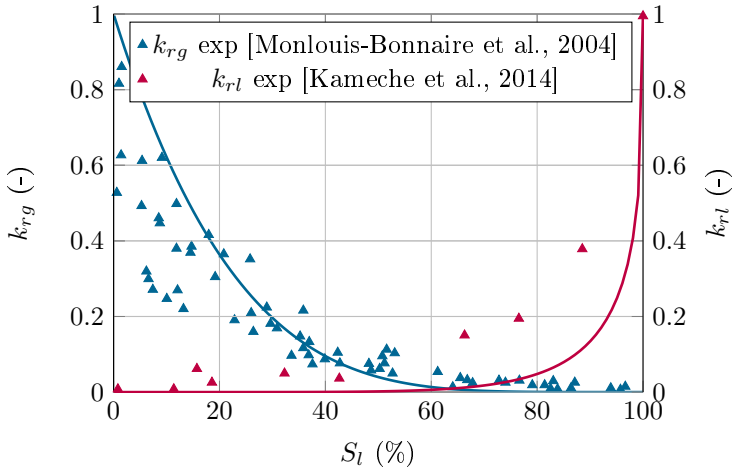

Figure 6: Relative gas/liquid water permeability versus degree of saturation.

4.3 Identification of the Intrinsic Permeability

Following the determination of the parameters defining the desorption curve and the variation of the relative permeability, the intrinsic permeability of gas k_g and liquid k_l must be identified. These two parameters can be obtained from a drying test. An inverse analysis is necessary for this purpose. The results obtained using the model proposed in this paper are compared with the experimental results reported by [Granger, 1995] and the numerical results found with Mensi's water transfer model of [Mensi et al., 1988].

The example studies the mass loss due to drying in a cylindrical concrete specimen of 16 cm in diameter. A 3-D calculation is performed since the hydric model is currently only implemented in a 3-D version in the Cast3M code. The parameters k_g and k_l are defined in such a way that the simulation of the mass loss can match, as precisely as possible, the experimental evolution [Granger, 1995] and the evolution obtained with Mensi's model [Mensi et al., 1988], on the one hand, and the moisture profiles on the other hand. In order to simplify the problem and reduce the number of elements in the mesh, a quarter of the sample is modeled. The

dimensions and the finite element mesh are shown in Figure 7.

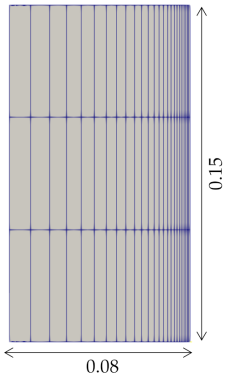

Figure 7: Geometrical characteristics and mesh of the cylindrical concrete sample (XZ plane) (dimensions in m).

In terms of hydric boundary conditions, the initial mass of liquid water in the concrete cylinder was 117.2 kg/m^3. The sample is subjected to drying at 47.5 % relative humidity for 2 years, which corresponds to an equivalent liquid mass of 52.6 kg/m^3. Since the liquid pressure, p_l, is the state variable chosen in the hydric transfer model, the initial equivalent liquid pressure in the concrete and that imposed externally at each time step are presented in Figure 8. The liquid pressure gradient existing between the environment (outside) and the concrete (inside) causes the drying by movement of the water in the sample. Note that the test was performed at room temperature.

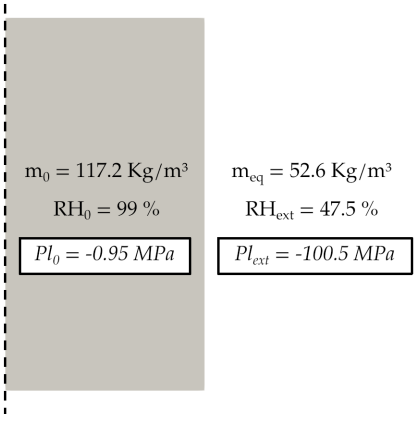

Figure 8: Hydric boundary conditions.

The different parameters used in this simulation are listed in Table 2.

It is necessary to reproduce the drying velocity and the global mass loss of the concrete correctly over time. Different values are assigned to the two intrinsic permeabilities k_g and k_l until the experimental profile given

Table 2: Parameters for concrete.

Symbol	Value	Unit
ϕ	0.12	-
M_{shr0}	13	MPa
m_{vgn}	0.35	-
n_{vgn}	1.1	-
q	0.5	-
p	4.5	-
T	293	K
T_0	293	K
T_{kvgn}	313	K

in [Granger, 1995] and the ones obtained numerically using the hydric model [Mensi et al., 1988] are found. As shown in Figure 9, for k_g equal to 1.5e-17 m^2 and k_l equal to 2.7e-21 m^2, the proposed water transfer model can reproduce the liquid mass loss over time. In addition, the drying rate is well calculated.

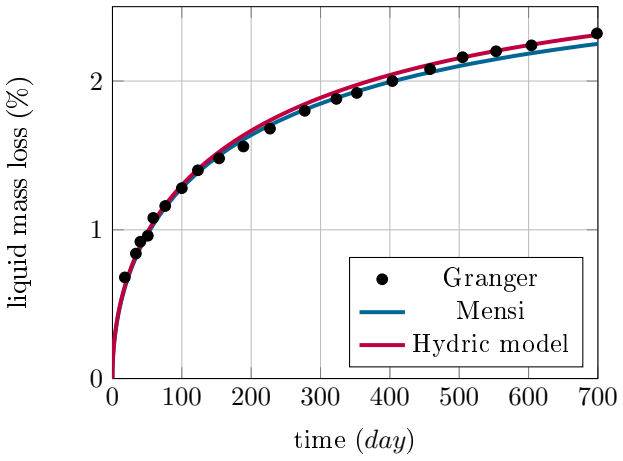

Figure 9: Global liquid mass loss (%) as a function of time (day).

An additional step is required to verify that the parameters have been correctly determined. During the drying process, the evolution of the liquid mass from the outer surface to the core of the sample is studied for different drying times. Figure 10 demonstrates that the proposed water transfer model is able to reproduce the liquid mass profile obtained experimentally by [Granger, 1995] and numerically by Mensi's model [Mensi et al., 1988] at different drying times. The liquid mass fields obtained for different time steps are shown in Figure 11. Thus, the hydric model using the liquid pressure p_l as a state variable and following the proposed calibration procedure is able to reproduce the experimental points correctly.

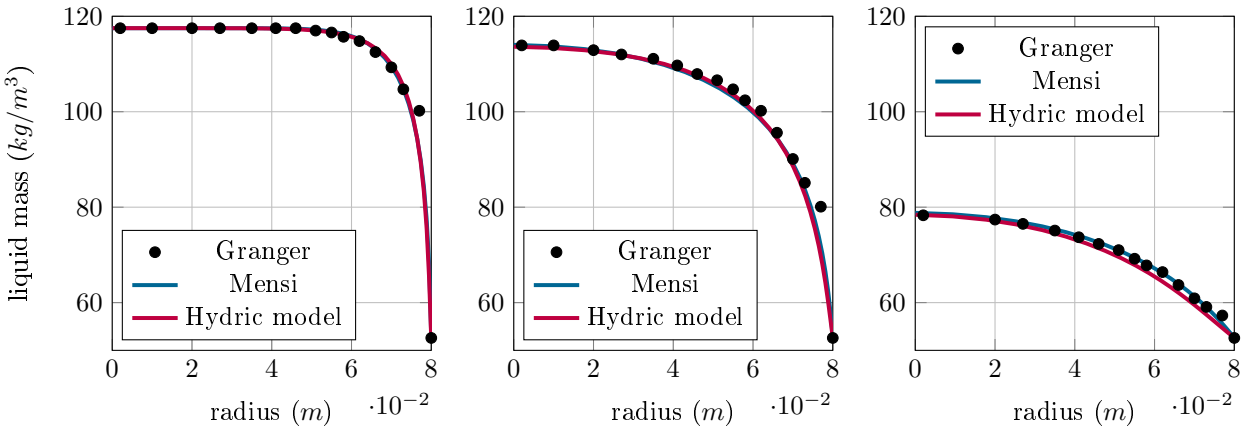

Figure 10: liquid mass in kg/m^3 as a function of radius in a 16 cm diameter specimen after (a) 3 days (b) 28 days (c) 460 days of drying at 50 % RH.

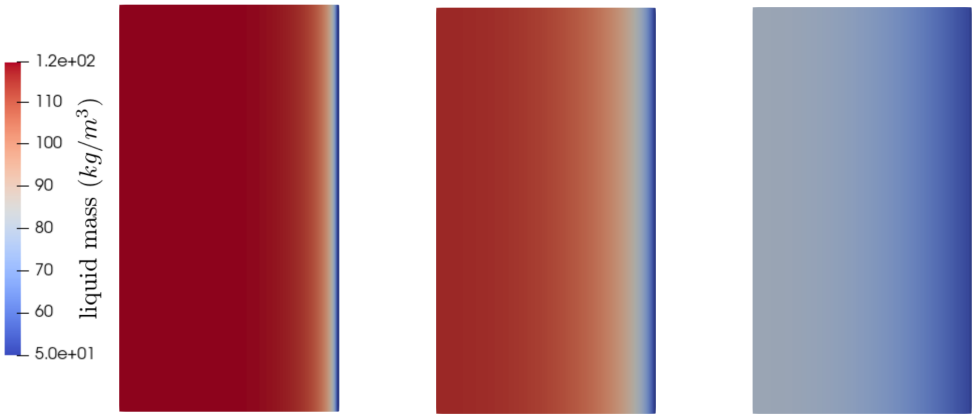

Figure 11: liquid mass field m_l (a) 3 days (b) 28 days (c) 460 days.

4.4 Validation of the Water Transfer Model in Temperature

After a detailed description of the calibration procedure used to assess the parameters used for the unsaturated problem at ambient temperature, this section aims to validate the capacity of the proposed hydric model to work in temperature, with a weakly coupled thermal transfer model.

4.4.1 Presentation of the Thermo-Hydric Test: the MAQBETH Mock-up

The application presented is used as a validation study of the proposed water transfer model. The simulated results are compared in detail with the experimental and numerical results found in [Bary et al., 2012] and carried out on the MAQBETH structure. This model uses a reinforced concrete hollow cylinder. The inner and outer diameters are 100 and 220 cm, respectively. The hollow concrete cylinder is 300 cm high. The cylinder is placed on a 60 mm thick wooden plate and its top part has a 200 mm thick insulation layer and an

additional wooden layer that is 30 mm thick. The geometrical characteristics of the hollow concrete cylinder and the schematic description of the experimental conditions are presented in Figure 12.

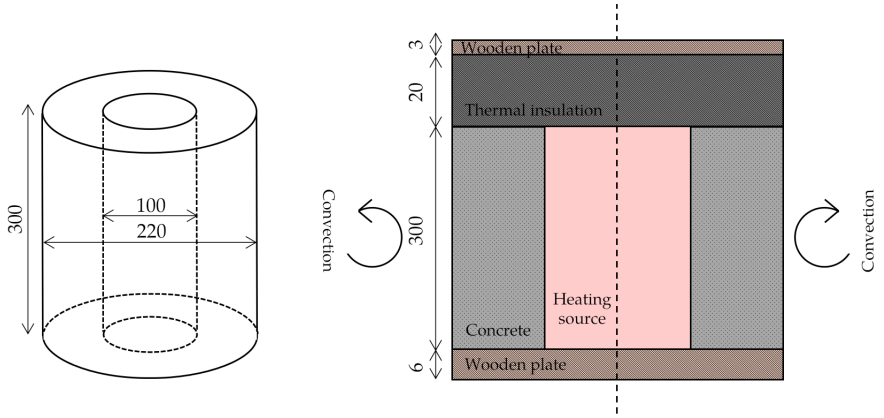

Figure 12: Geometrical characteristics of the hollow concrete cylinder (MAQBETH mock-up) (a) 3D view (b) boundary conditions (dimensions are in cm).

Numerically, a slice of the hollow cylinder is studied. This option is selected to reduce the number of finite elements used in the mesh and, thus, to speed up the calculation (see Figure 13-a).

For the thermal boundary conditions, there is a heating source in the internal area of the structure, which imposes the temperature change, as shown in Figure 13-b. The heating source inside the hollow cylinder causes a large temperature gradient in the concrete. To correctly model this gradient and converge the calculation, a fine mesh is applied near the two vertical sides of the cylinder. No gradient is applied in the height of the cylinder since a thermal insulator is present and zero flow is assumed (see Figure 13-a).

Regarding the hydric boundary conditions, a constant vapor pressure, p_v, is imposed on the inner and outer sides of the structure. This pressure was set at 2500 Pa. Since the state variable of the hydric model is the liquid pressure, p_l, the Kelvin-Laplace law is used to convert it to equivalent liquid pressure. Thus, the imposed liquid pressure, p_l, is expressed according to the vapor to ensure a constant vapor pressure p_v equal to 2500 Pa at each time step. The thermal and hydric boundary conditions applied to the 3-D model are presented in Figure 13.

The heat and water transfer boundary conditions and parameters are summarized in Tables 4 and 3, respectively.

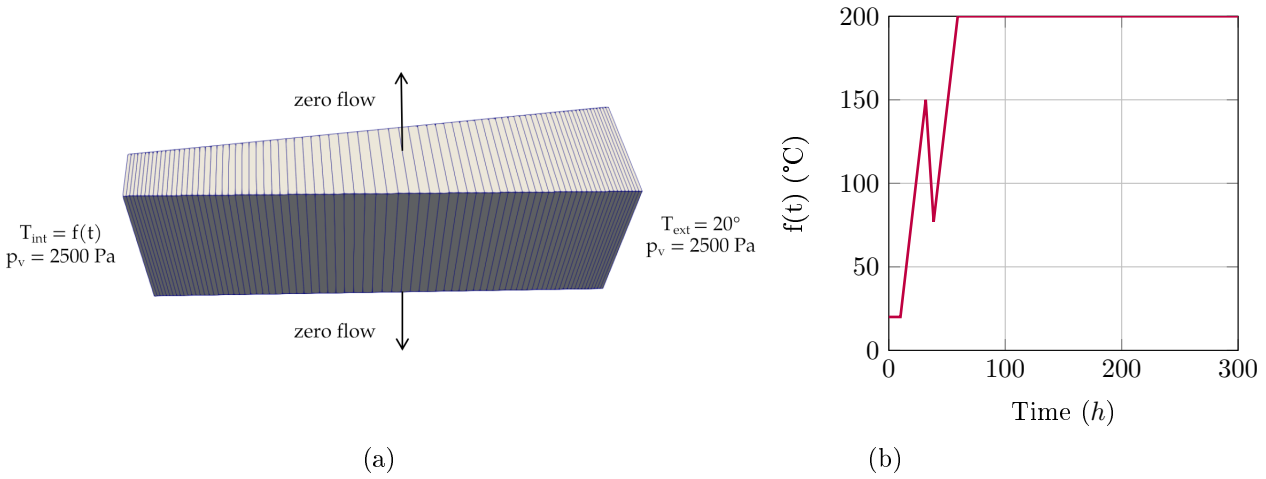

(a) (b)

Figure 13: (a) Boundary conditions applied to the 3-D model (b) Thermal loading history on the inner surface.

4.4.2 Numerical Results

The experimental data (points) [Ranc et al., 2003] and numerical profiles (lines) of the radial temperature at different times are presented in Figure 14. The dashed lines refer to the numerical results obtained in [Bary et al., 2012] and the solid lines correspond to our calculation. The distance varies between 0 and 0.6 m. These values represent the thickness of the hollow cylinder with 0 as the inner surface and 0.6 as the outer surface. It can be seen that the numerical curves are close to the experimental data. A slight deviation can be observed between the results obtained here and those given experimentally or found with the numerical model of [Bary et al., 2012]. This may be due to the approximation of the thermal conductivity in the material. Despite this deviation, the results are acceptable and the model can be used to provide a good representation of the temperature inside the material at each time step of the water mass transfer model.

As the state variable of the hydric transfer model presented is the liquid pressure, p_l, the evolution of its radial profiles must be studied. As a result of the temperature variation in the inner zone of the hollow cylinder due to thermal loading, the imposed liquid pressure, p_l, on the boundaries will also vary, maintaining a constant vapor pressure, p_v, of 2500 Pa. Figure 15 shows that the liquid pressure, p_l, at the inner surface of the cylinder decreases as the temperature increases. This decrease leads to a progressive diminution of p_l in the radial direction of the structure.

Moreover, the example also supplies the vapor pressure evolution. Figure 16 gives the profiles of p_v as a function of the hollow cylinder thickness. At the beginning of the temperature increase within the MAQBETH structure, the peak of the vapor pressure is located close to the inner surface. This can be explained by the

Table 3: Thermo-hydro boundary conditions and parameters for MAQBETH concrete.

Symbol	Value	Unit
ϕ	0.1	-
RH	97	%
T_{int}	f(t)	$°C$
T_{ext}	20	$°C$
T_{ref}	20	$°C$
ρ_{ref}	2408	kg/m^3
λ_{ref}	2.1	$W/(m.K)$
$c_{p\ ref}$	913	$J/(kg.K)$
h	10	$W/(m^2.°C)$
p_{l0}	-5.5	MPa
$p_{l,ext}$	-17	MPa
$p_{l,int,0}$	-17	MPa
M_{shr0}	13	MPa
m_{vgn}	0.35	-
n_{vgn}	1.1	-
q	0.5	-
p	4.5	-
k_l	$1*10^{-23}$	m^2
k_g	$2.7*10^{-18}$	m^2

Table 4: Thermal parameter functions used in the simulations.

Symbol	Expression	Unit
ρ	$\rho_{ref} * \left(1 - 3.25e^{-3}(T - T_{ref})^{0.5}\right)$	kg/m^3
λ	$\lambda_{ref} * \left(1 - 3.26e^{-3}(T - T_{ref})\right)$	$W/(m.K)$
c_p	$c_{p\ ref} * \left(1 - 6.65e^{-4}(T - T_{ref})\right)$	$J/(kg.K)$

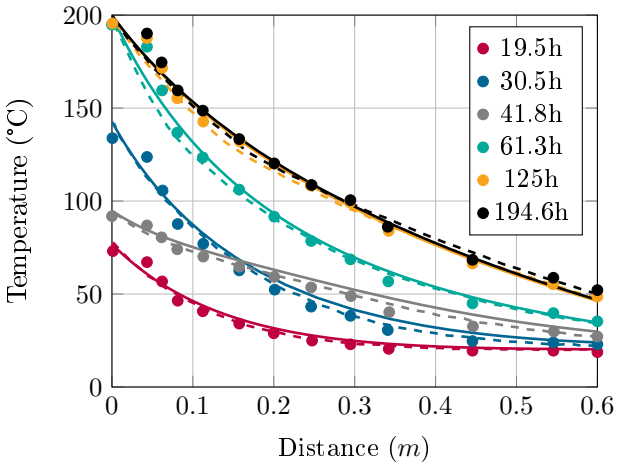

Figure 14: Comparison of radial temperature profiles at different times (hours) between experimental measurements (points), the numerical model of [Bary et al., 2012] (dashed lines) and the numerical model proposed here (solid lines).

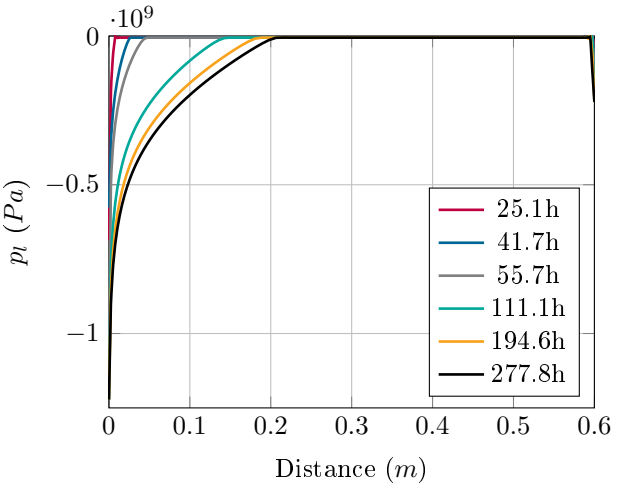

Figure 15: Profiles of liquid pressure p_l as a function of the radial distance from the inner surface at different times (hours).

evaporation of liquid water induced by an incoming heat flow than is faster than the outgoing vapor flow. As can be seen, the model gives the value of the peak found experimentally. The simulations become more consistent with the experimental data as the temperature increases. Over time, the peak of p_v decreases and moves towards the outside of the concrete cylinder, because the vapor escapes more easily to the center of the cylinder than to the outside, due to the slow desaturation of the outer zone. The curves obtained using the model proposed in this paper are close to those obtained with the numerical hydric model of [Bary et al., 2012].

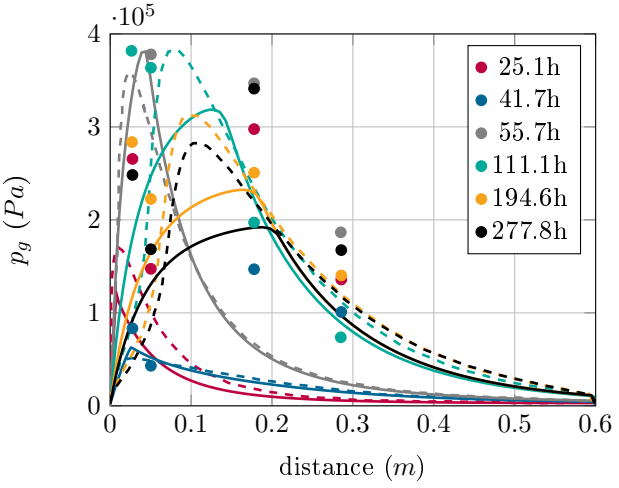

Figure 16: Comparison of radial total gas pressure profiles at different times (hours) obtained by the experimental measurements (points) and the numerical model of [Bary et al., 2012] (dashed lines) with vapor pressure profiles obtained by the numerical model proposed here (solid lines).

The vapor pressure field along the thickness of the cylinder is displayed in Figure 17. As can be seen, and

as interpreted from the curves in Figure 16, the maximum vapor pressure is initially situated near the inner surface of the cylinder. Over time, the zone of maximum vapor pressure moves toward the outside surface of the cylinder, causing a decrease in the highest value of p_v.

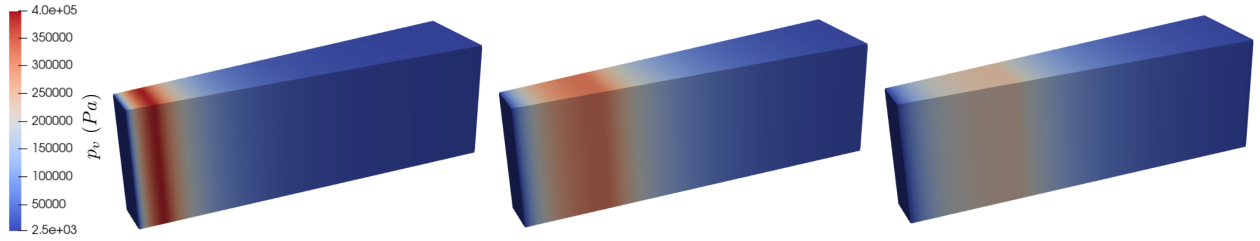

(a) (b) (c)

Figure 17: Vapor pressure p_v field (a) 55.7h (b) 111.1h (c) 194.6h.

This case of study shows that a simplified water transfer model based only on the liquid pressure is able to model a multi-physics thermo-hydric problem.

4.5 Application to a Case Study Involving Both Positive and Negative Liquid Pressures at the Boundaries

In this last subsection, the ability of the hydric transfer model to handle complex hydric conditions is examined. This study deals with the modeling of water transfer in a tunnel similar to the ones usable to store radioactive wastes. It aims to determine the evolution of the liquid pressure, p_l, in the drying and re-saturation phases of the tunnel. In addition, the re-saturation time of the soil and its return to the initial state is calculated based on adequate numerical modeling. This research is essential to improve knowledge of the short and long-term thermo-hydro-mechanical behavior of radioactive waste storage tunnels.

4.5.1 Geometry and Boundary Conditions

The geometry and material properties of nuclear waste storage structures proposed by the French Agency for Nuclear Waste Management (Andra) are used in this example. They are composed of multiple tunnels located 500 m below the ground surface. The tunnels are surrounded by Callovo Oxfordian (COX) soil. In the tunnel construction, a hole of 5.05 m radius is excavated at a depth of 500 m. Following the excavation, two layers of concrete are placed. The first layer of concrete represents a 0.2 m thick compressible material to absorb the displacements due to soil convergence. The second layer forms the principal part of the tunnel. It consists of a concrete layer 8.7 m in internal diameter and 0.5 m thick. As a result of the excavation in the soil, two elliptical excavation disturbed zones (EDZ) develop around the tunnel. These two zones can significantly influence the

phenomenon of soil saturation and de-saturation because of their high permeability. Thus, three soil layers with different water transfer parameters are modeled in the simulation. The dimensions of the tunnel and EDZ are shown in Figure 18-a. The vertical liquid pressure soil boundary conditions are positive. They are imposed far enough from the tunnel to have no influence on the kinetics of water transfers. Vertically, two planes of symmetry are modeled by a null flow.

The calculation is composed of two phases. First, after placing of the concrete, a drying phase is considered (ventilation). A relative humidity, RH, of 50 %, corresponding to a liquid pressure of -95 MPa, is imposed on the internal surface of the tunnel. Then, after 100 years, the tunnel is closed and the phase of re-saturation of the underground structure begins (no more ventilation). A three-dimensional analysis is performed using CAST3M. As shown in Figure 18-b, only half of the underground structure is investigated thanks to the vertical symmetry of the geometry. A ground width of 25 m is considered in the simulation. This value corresponds to half the distance between two parallel tunnels. The finite element mesh and water boundary conditions are given in Figure 18-b.

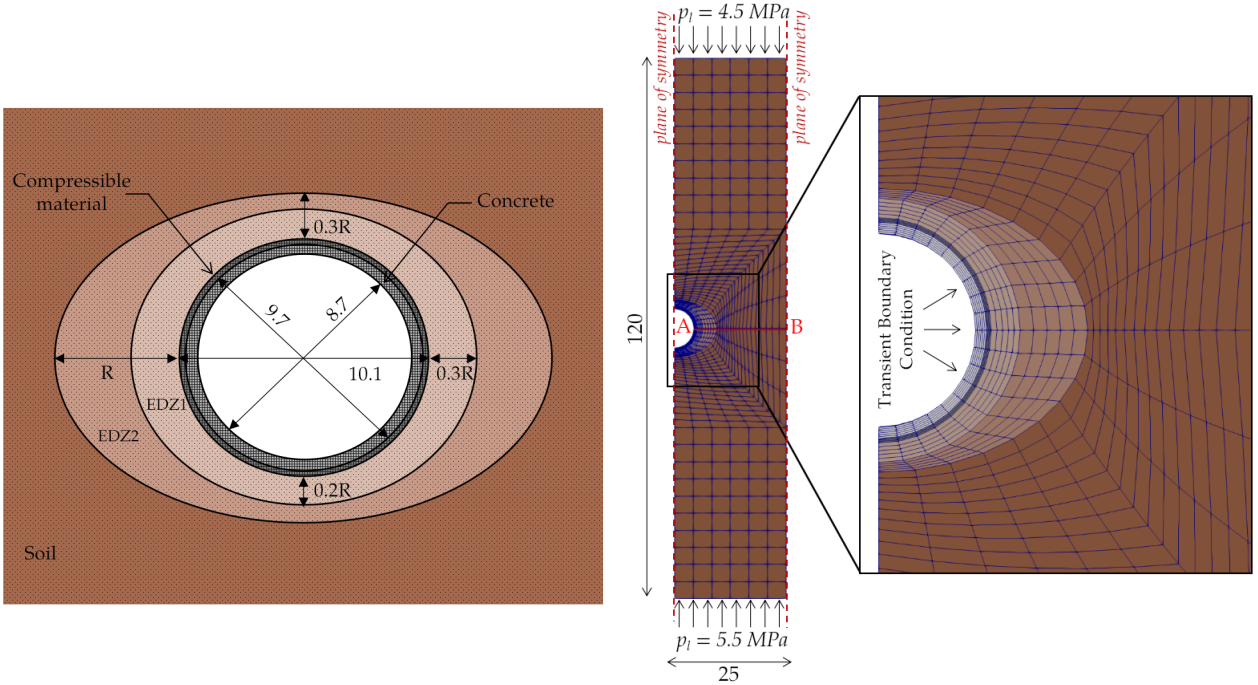

Figure 18: (a) Geometrical characteristics, (b) mesh and boundary conditions of the tunnel.

The parameters of the hydric model for the concrete and the damaged/undamaged soil were provided by Andra. The permeability parameters are within the ranges defined by [Gatmiri et al., 2011]. They are summarized in

Table 5.

This application focuses only on the moisture transfer and not on the mechanical load applied by the soil. It is not a poro-mechanical model. This means that the solid is assumed to be undeformable, which can lead to a poor estimation of the real re-saturation kinetics. As explained in the conclusion, the coupling of this water mass transfer model with a thermo-mechanical model of soil and concrete is the next step of our research project. Also, for the sake of simplification, a constant temperature, T, of $20°C$ is maintained throughout the simulation, which should not be the case in reality. The numerical results of this first prediction must therefore be seen more as proof that the model is indeed capable of simultaneously taking both positive and negative pressure boundary conditions into account, rather than as a realistic prediction.

Table 5: Hydric parameters provided by ANDRA.

Parameter	**Concrete**	**EDZ1**	**EDZ2**	**Soil**
ϕ (-)	0.135	0.18	0.18	0.18
k_l (m^2)	$9.59e^{-18}$	$9.59e^{-17}$	$9.59e^{-19}$	$9.59e^{-21}$
k_g (m^2)	$1.5e^{-17}$	$9.59e^{-14}$	$9.59e^{-16}$	$9.59e^{-20}$
M_{shr0} (MPa)	19.6	17.7	17.7	17.7
m_{vgn} (-)	0.33	0.34	0.34	0.34
n_{vgn} (-)	1.5	1.52	1.52	1.52

4.5.2 Interpretation of Results

Stage 1: 0-100 years (ventilation)

Initially, since the excavation disturbs the soil, the liquid pressure, p_l, in the damaged zone (EDZ) becomes negligible. Furthermore, during the placement of the two concrete layers, the liquid pressure, p_l, within the tunnel is assumed to be zero. This assumption is based on the massive nature of the concrete structure, which makes it possible to assume an initial liquid pressure close to zero in the concrete and the EDZ.

Figure 19 represents the evolution of the liquid pressure field in the tunnel and soil at the time of concrete placement, after 10 years, and after 100 years of ventilation. As can be seen, at 100 years, a desaturation of the concrete and soil occurs. It is caused by the 50% relative humidity applied in the ventilation area (corresponding to a liquid pressure equal to -95 MPa). The pressure difference between the center of the excavation and the tunnel/soil structure attracts the water contained in the pores to the external surface of the tunnel. This water will evaporate, desaturating the concrete and the EDZ. This phenomenon causes a decrease in the pressure of the liquid inside the underground structure.

Figure 20 provides a quantitative analysis of the evolution of liquid pressure over time in concrete and soil along line AB in Figure 18-b.

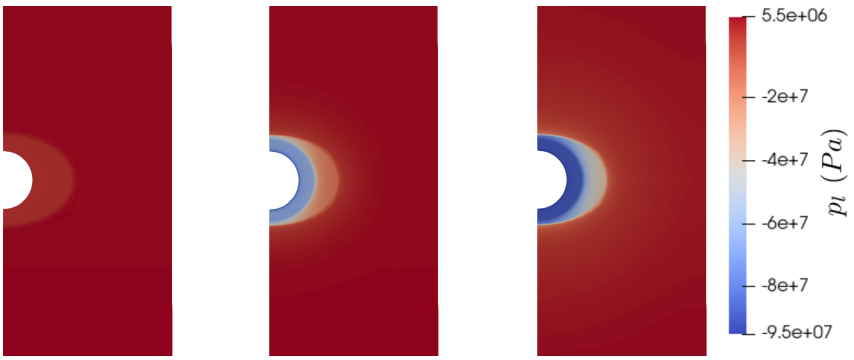

Figure 19: Variation of the liquid pressure p_l field in and around the tunnel after (a) excavation and concrete placement (b) 10 years (c) 100 years.

In one year, the desaturation affects the concrete tunnel and the two EDZ caused by the excavation. It then propagates slowly toward the undamaged soil. As time passes, the underground structure gradually dries. However, because of the high permeability of EDZ1, the liquid pressure in this zone varies rapidly and a negligible liquid pressure gradient is observed. This gradient grows in zone EDZ2 and the undamaged soil. After 100 years, the concrete is almost in moisture equilibrium with the ventilated area.

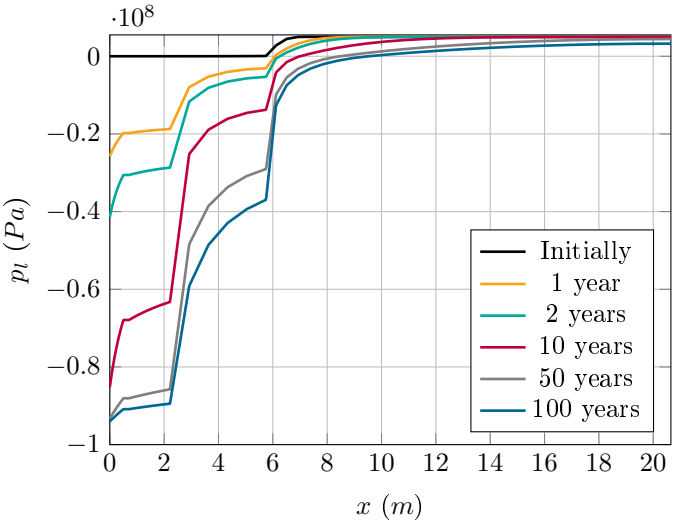

Figure 20: Evolution of the liquid pressure, p_l, along the horizontal line AB (phase 1: ventilation).

Stage 2: After 100 years, Re-saturation

After 100 years, the ventilation is stopped and the re-saturation phase of the underground structure begins. The initial boundary condition of 50 % relative humidity in the tunnel is replaced by a zero flow condition. Consequently, an increase occurs in liquid pressures in the concrete and soil. Figure 21 shows the liquid

pressure evolution in the tunnel and surrounding soil for different periods. The time required for the pressure to become positive (end of re-saturation) in the tunnel is reached at 7143 years. Thereafter, the liquid pressure continues to progress positively until equilibrium with natural water pressure is reached. The time at which the pressure becomes almost uniform is around 18000 years.

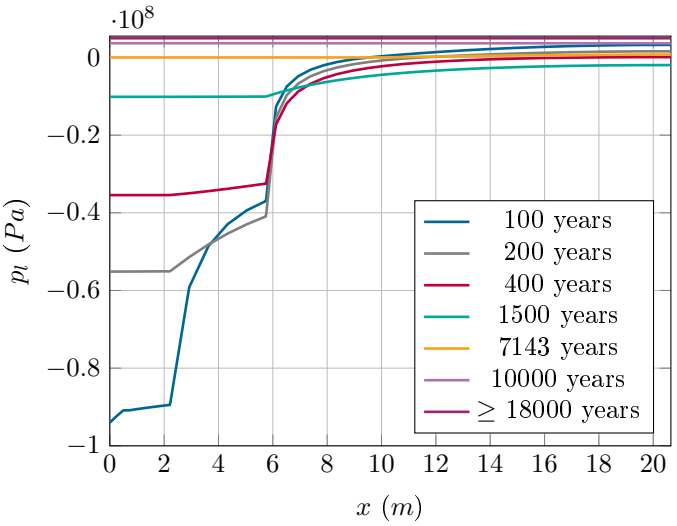

Figure 21: Evolution of the liquid pressure, p_l, along the horizontal line AB (phase 2: re-saturation).

The variation of liquid pressure, p_l, over time is illustrated in Figure 22. Only the positive part of p_l is shown in order to visualize the re-saturation process of the underground structure clearly.

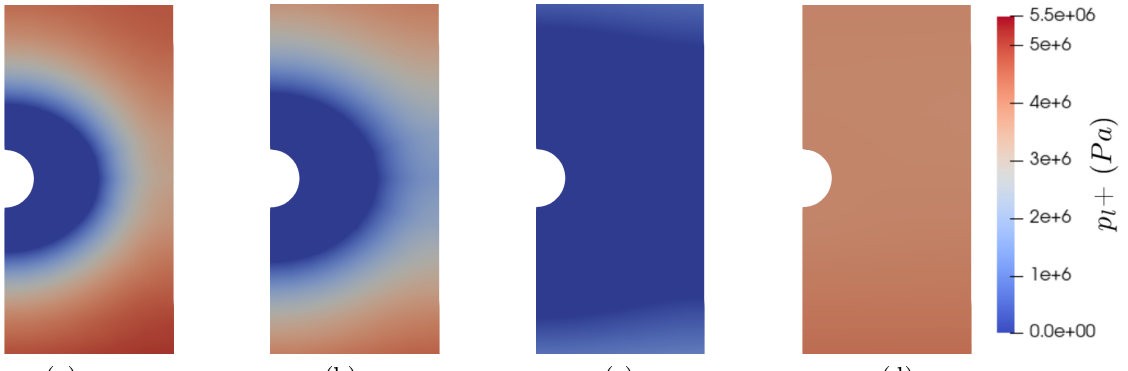

Figure 22: Variation of the liquid pressure, p_l, in and around the tunnel after (a) 100 years (b) 200 years (c) 1500 years (d) 18000 years.

This last application shows that this water mass transfer model, using only liquid water pressure as a state variable, is able to capture the continuous displacement of the boundary between the drying zones with negative pressures and the saturated zones with positive liquid water pressure.

5 Conclusions and Perspectives

This paper proposes a simplified hydric transfer model with the liquid pressure of water as single state variable. The formulation of this model is based on two main assumptions :

- Vapor pressure remains large compared to dry air pressure. This assumption stays realistic as long as the porous medium is not too dry. This means that the porous material has an initial degree of saturation high enough to consider that its fine pores are saturated with liquid water and that they constitute the major part of the porosity, thus supplying a large quantity of vapour during the transient problem. A means of verifying this assumption is to compute the error that occurs after the calculation is completed. The maximum mass transfer error can be defined as the ratio between the mass flow of dry air and the mass flow of water in its two phases, liquid and vapor. The validity of this first assumption is demonstrated by comparing it with the experimental results of two drying problems: one a small specimen of concrete drying to 47.5 %RH at 20°C (Granger tests), and another one at higher temperatures, up to 200°C (MAQBETH mock-up).

- Vapor and liquid pressures of water are related by a thermodynamic law assuming that the specific volume of vapor is non-negligible compared to the specific volume of water. This assumption is not a simplification, but a better description of the physics.

The resulting water conservation law is derived from macroscopic laws permitting the expression of vapor pressure and degree of saturation as functions of liquid pressure (such as the Kelvin-Laplace law and sorption/desorption curves). The main interest of this model is to provide a continuous description of water transport in saturated (positive liquid pressure) and unsaturated (negative liquid pressure) media, which allows boundary conditions of drying and boundary conditions of positive pressure to be considered simultaneously in the same problem. This is done without resorting to a coupled mass transfer problem of dry air, vapor and liquid. This simplification enables a rapid implementation based on a simple thermal non-linear analogy (as illustrated in the tunnel case study). Moreover, as shown in our second case of study, this model is able to consider transfer at high temperatures. Three other assumptions are used in this paper. They are not strictly necessary but are made for the sake of simplification:

- First, the solid skeleton of porous media is assumed to be undeformable to avoid a full poro-mechanical formulation. However, this context is not mandatory: if the deformation of the solid was considered to compute the hydro-mechanical behavior of a partially saturated structure, the benefit of this model could be kept, leading to a "displacement-liquid pressure" formulation (with 4 state variables in 3D, namely the displacement (u, v, w) and the liquid pressure P_l), saving the cost of calculating the vapor pressure,

p_v, and the gas pressure, p_a.

- Second, the heat transfer equation has been decoupled from the mass transfer equation, again for simplicity. However here again, the simplification is not mandatory because, as with poro-mechanics, the fully coupled formulation of this model with the heat transfer equation would save the calculation cost of the same two state variables (P_v and P_a).

- Third, the hysteresis of the water retention curves is neglected. To consider this aspect, the present model should be coupled with a hysteresis model capable of changing the slope of the retention curve according to the sign of the liquid mass variation. This is a possible perspective for development.

One of the main perspectives of (and reasons for) of this work is to couple this water transfer model to the mechanical behavior of the porous media by considering, on the one hand, the deformability of the solid skeleton and, on the other hand, the possible variation of permeability induced by mechanical nonlinearities, such as plasticity and nonlocal damage.

Acknowledgment

This research was partially supported by the the French agency for nuclear waste management ANDRA and the French National Research Agency (ANR-PIA) under the MACENA research program 11-RSNR-0012 (Control of nuclear vessel in accident conditions).
We are also grateful to CEA for providing the finite element code CASTEM (www.cast3m.cea.fr).

References

S Arrhenius. Les oscillations séculaires de la température à la surface du globe terrestre. *Ciel et Terre*, 20: 411–419, 1900.

V Baroghel-Bouny, M Mainguy, T Lassabatere, and O Coussy. Characterization and identification of equilibrium and transfer moisture properties for ordinary and high-performance cementitious materials. *Cement and concrete research*, 29(8):1225–1238, 1999. doi: https://doi.org/10.1016/S0008-8846(99)00102-7.

EP Barrett, LG Joyner, and PP Halenda. The determination of pore volume and area distributions in porous substances. i. computations from nitrogen isotherms. *Journal of the American Chemical society*, 73(1): 373–380, 1951. doi: https://doi.org/10.1021/ja01145a126.

B Bary, G Ranc, S Durand, and O Carpentier. A coupled thermo-hydro-mechanical-damage model for concrete subjected to moderate temperatures. *International journal of heat and mass transfer*, 51(11-12):2847–2862, 2008. doi: https://doi.org/10.1016/j.ijheatmasstransfer.2007.09.021.

B Bary, M VG De Morais, S Poyet, and S Durand. Simulations of the thermo-hydro-mechanical behaviour of an annular reinforced concrete structure heated up to 200 °c. *Engineering structures*, 36:302–315, 2012. doi: https://doi.org/10.1016/j.engstruct.2011.12.007.

ZP Bažant and LJ Najjar. Drying of concrete as a nonlinear diffusion problem. *Cement and concrete research*, 1(5):461–473, 1971. doi: https://doi.org/10.1016/0008-8846(71)90054-8.

ZP Bažant and W Thonguthai. Pore pressure and drying of concrete at high temperature. *Journal of the Engineering Mechanics Division*, 104(5):1059–1079, 1978. doi: https://doi.org/10.1061/JMCEA3.0002404.

J. Carette, Fr. Soleilhet, F. Benboudjema, X. Ma, G. Nahas, K. Abahri, A. Darquennes, and R. Bennacer. Identifying the mechanisms of concrete drying: An experimental-numerical approach. *Construction and Building Materials*, 230:117001, 2020. doi: https://doi.org/10.1016/j.conbuildmat.2019.117001.

CEA. Cast3m. *Commissariat à l'Energie Atomique*, 2016.

W Chen, J Liu, F Brue, F Skoczylas, CA Davy, X Bourbon, and J Talandier. Water retention and gas relative permeability of two industrial concretes. *Cement and Concrete Research*, 42(7):1001–1013, 2012. doi: https://doi.org/10.1016/j.cemconres.2012.04.003.

O Coussy. *Poromechanics*. John Wiley & Sons, 2004.

M VG de Morais, B Bary, G Ranc, SD Pont, and S Durand. Comparative analysis of coupled thermo-hydro-mechanical models for concrete exposed to moderate temperatures. *Numerical Heat Transfer, Part A: Applications*, 55(7):654–682, 2009. doi: https://doi.org/10.1080/10407780902821516.

Eurocode2. Eurocode 2: Design of concrete structures—part 1-1: General rules and rules for buildings. *London: British Standard Institution*, 2004.

A Feraille-Fresnet. *Le role de l'eau dans le comportement à haute température des bétons*. PhD thesis, Marne-la-vallée, ENPC, 2000.

B Gatmiri, C Auvray, P Besuel, S Chanchol, C Dascalu, P De Buhan, P Delage, J Desrues, L Dormieux, R Giot, et al. Synthese générale du programme 2007-2011 du groupement de laboratoire géomécanique. Technical report, Technical report, ANDRA, 2011.

D Gawin, CE Majorana, and BA Schrefler. Numerical analysis of hygro-thermal behaviour and damage of concrete at high temperature. *Mechanics of Cohesive-frictional Materials: An International Journal on Experiments, Modelling and Computation of Materials and Structures*, 4(1):37–74, 1999. doi: https://doi.org/10.1002/(SICI)1099-1484(199901)4:1<37::AID-CFM58>3.0.CO;2-S.

ZX Gong, B Song, and Arun S Mujumdar. Numerical simulation of drying of refractory concrete. *Drying Technology*, 9(2):479–500, 1991. doi: https://doi.org/10.1080/07373939108916677.

L Granger. *Comportement différé du béton dans les enceintes de centrales nucléaires: analyse et modélisation*. PhD thesis, Ecole Nationale des ponts et Chaussées, 1995.

H Kallel, H Carré, C Laborderie, B Masson, and NC Tran. influence of moisture and temperature on mechanical properties of the concrete. In *9th International Conference on Fracture Mechanics of Concrete and Concrete Structures, FraMCoS-9: Proceedings Volume*, page 9. IA-FraMCoS, 2016.

ZA Kameche, F Ghomari, M Choinska, and A Khelidj. Assessment of liquid water and gas permeabilities of partially saturated ordinary concrete. *Construction and Building Materials*, 65:551–565, 2014. doi: https://doi.org/10.1016/j.conbuildmat.2014.04.137.

LJ Klinkenberg. The permeability of porous media to liquids and gases. *Am. Petrol. Inst., Drilling and Production Practice*, 2:200–213, 1941.

AV Luikov. Systems of differential equations of heat and mass transfer in capillary-porous bodies. *International Journal of Heat and mass transfer*, 18(1):1–14, 1975. doi: https://doi.org/10.1016/0017-9310(75)90002-2.

M Mainguy, O Coussy, and R Eymard. *Modélisation des transferts hydriques isothermes en milieu poreux. application au séchage des matériaux à base de ciment*. Number OA 32. 1999.

M Mainguy, O Coussy, and V Baroghel-Bouny. Role of air pressure in drying of weakly permeable materials. *Journal of engineering mechanics*, 127(6):582–592, 2001. doi: https://doi.org/10.1061/(ASCE)0733-9399(2001)127:6(582).

R Mensi, P Acker, and A Attolou. Séchage du béton: analyse et modélisation. *Materials and structures*, 21 (1):3–12, 1988.

JP Monlouis-Bonnaire, J Verdier, and B Perrin. Prediction of the relative permeability to gas flow of cement-based materials. *Cement and Concrete Research*, 34(5):737–744, 2004. doi: https://doi.org/10.1016/S0008-8846(03)00071-1.

JR Philip and DA De Vries. Moisture movement in porous materials under temperature gradients. *Eos, Transactions American Geophysical Union*, 38(2):222–232, 1957. doi: https://doi.org/10.1029/TR038i002p00222.

C. Pohl, V. Šmilauer, and J. Unger. A three-phase transport model for high-temperature concrete simulations validated with x-ray ct data. *Materials*, 14(17):5047, 2021. doi: https://doi.org/10.3390/ma14175047.

S Poyet. Experimental investigation of the effect of temperature on the first desorption isotherm of concrete. *Cement and Concrete Research*, 39(11):1052–1059, 2009. doi: https://doi.org/10.1016/j.cemconres.2009.06.019.

H Ranaivomanana. *Tranferts dans les milieux poreux réactifs non saturés: application à la cicatrisation de fissure dans les matériaux cimentaires par carbonatation.* PhD thesis, Université de Toulouse, Université Toulouse III-Paul Sabatier, 2010.

G Ranc, J Sercombe, and S Rodrigues. Comportement à haute température du béton de structure: Impact de la fissuration sur les transferts hydriques. *Revue française de génie civil*, 7(4):397–424, 2003.

K Raznjevic and R Podhorsky. *Tables et diagrammes termodynamiques.* Eyrolles Paris, 1970.

LA Richards. Capillary conduction of liquids through porous mediums. *Physics*, 1(5):318–333, 1931. doi: https://doi.org/10.1063/1.1745010.

V. Šmilauer, P. Havlásek, T. Gasch, A. Delaplace, D. E-M Bouhjiti, F. Benboudjema, M. Briffaut, F. Kanavaris, and M. Azenha. Hygro-mechanical modeling of restrained ring test: Cost tu1404 benchmark. *Construction and Building Materials*, 229:116543, 2019. doi: https://doi.org/10.1016/j.conbuildmat.2019.07.269.

M Thiery, V Baroghel-Bouny, N Bourneton, G Villain, and C Stéfani. Modélisation du séchage des bétons: analyse des différents modes de transfert hydrique. *Revue européenne de génie civil*, 11(5):541–577, 2007.

HR Thomas and MR Sansom. Fully coupled analysis of heat, moisture, and air transfer in unsaturated soil. *Journal of Engineering Mechanics*, 121(3):392–405, 1995. doi: https://doi.org/10.1061/(ASCE)0733-9399(1995)121:3(392).

M Th Van Genuchten. A closed-form equation for predicting the hydraulic conductivity of unsaturated soils. *Soil science society of America journal*, 44(5):892–898, 1980. doi: https://doi.org/10.2136/sssaj1980.03615995004400050002x.

R Witasse, JF Georgin, and JM Reynouard. Nuclear cooling tower submitted to shrinkage; behaviour under weight and wind. *Nuclear Engineering and Design*, 217(3):247–257, 2002. doi: https://doi.org/10.1016/S0029-5493(02)00160-7.

677 Y Xi, ZP Bažant, L Molina, and HM Jennings. Moisture diffusion in cementitious materials moisture capac-
678 ity and diffusivity. *Advanced Cement Based Materials*, 1(6):258–266, 1994. doi: https://doi.org/10.1016/
679 1065-7355(94)90034-5.

680 X. Zhang, C. Shu, M. Fujii, Y. Wu, D. Sun, P. Ye, and Y. Bao. Numerical and experimental study on water-
681 heat-salt transport patterns in shallow bare soil with varying salt contents under evaporative conditions: A
682 comparative investigation. *Journal of Hydrology*, 621:129564, 2023. ISSN 0022-1694. doi: https://doi.org/
683 10.1016/j.jhydrol.2023.129564.